

# Single-Shot 360-Degree Cranial Deformity Detection System Using Digital Image Correlation

Shaogang Liu<sup>#</sup>, Long Yin<sup>#</sup>, Wei Yin, Yuzhen Zhang<sup>✉</sup>, Chao Zuo

**Abstract:** In this paper, a single-shot 360-degree cranial deformity detection system using digital image correlation (DIC) is presented to quickly obtain and detect accurate 3D data of infants' cranium. By introducing plane mirrors into a stereo 3D DIC measurement system, a multi-view 3D imaging model is established to convert 3D data from real and virtual perspectives into 360-degree 3D data of the tested infant cranium, achieving single-shot and panoramic 3D measurement. Experimental results showed that the performance and measurement accuracy of the proposed system can meet the requirements for cranial deformity detection, which provides a fast, accurate, and low-cost solution medically.

**Keywords:** single-shot measurement; 360-degree measurement; cranial deformity detection

## 1 Introduction

With the continuous improvement of people's living conditions, health problems have gradually become one of the most concerned daily topics, especially those related to infants. The cranial deformity is one of the main diseases that affect the normal development of infants, which is usu-

ally called flat head syndrome medically, including several abnormal head symptoms such as oblique head, short head, short oblique head, and boat head [1–4]. The flat head syndrome will affect the appearance of infants and may cause such problems as torticollis, uneven development of muscle tissue in cranium and visual nerves on both sides, and mental retardation. In severe cases, the structure of the brain cavity will be damaged, leading to problems with neurodevelopment and hindering intellectual development[5].

The cranial deformity is extremely harmful to the healthy growth of infants, and most of them will not recover automatically with matures physically. Without timely treatment, it will have a long-term impact greatly on children and accompany them for life. Therefore, when the infant cranium is in the rapid growth period, once the cranial deformity is diagnosed, an active and effective treatment should be taken[6, 7]. In most cases, the younger the child, the faster the treatment speed and the better its effect. Therefore, developing a quick and accurate intelligent detection equipment for infant cranial parameters to screen cranial deformity, which can effectively reduce the incidence of the flat

---

Manuscript received Dec. 31, 2021; revised Feb. 14, 2022; accepted Feb. 18, 2022. The associate editor coordinating the review of this manuscript was Dr. Liheng Bian. This work was supported by the National Natural Science Foundation of China (No. 62075096), Leading Technology of Jiangsu Basic Research Plan (No. BK20192003), National Defense Science and Technology Foundation of China (No. 2019-JCJQ-JJ-381), "333 Engineering" Research Project of Jiangsu Province (No. BRA2016407), Jiangsu Provincial "One Belt and One Road" Innovation Cooperation Project (No. BZ2020007), Fundamental Research Funds for the Central Universities (Nos. 30921011208, 30919011222 and 30920032101) and Open Research Fund of Jiangsu Key Laboratory of Spectral Imaging & Intelligent Sense (No. JS-GP202105).

Shaogang Liu, Long Yin, Wei Yin, Yuzhen Zhang and Chao Zuo are with School of Electronic and Optical Engineering, Nanjing University of Science and Technology, Nanjing 210094, China; Jiangsu Key Laboratory of Spectral Imaging & Intelligent Sense, Nanjing 210094, China; Smart Computational Imaging Laboratory (SCILab), Nanjing University of Science and Technology, Nanjing 210094, China and Smart Computational Imaging Research Institute (SCIRI) of Nanjing University of Science and Technology, Nanjing 210019, China.

✉ Corresponding author. Email: zyz\_1973@njjust.edu.cn

<sup>#</sup>Shaogang Liu and Long Yin are co-first authors of the article.

DOI: [10.15918/j.jbit1004-0579.2021.104](https://doi.org/10.15918/j.jbit1004-0579.2021.104)

head syndrome, is a major public health project worthy of popularization[8–11].

At present, the devices such as spreading caliper, 3D CT imaging, and handheld-based structured light scanners are mainly used to measure infants' head shape for cranial deformity detect medically. Among them, the spreading caliper is easy to use but low-accuracy and its detection data can't be used for the treatment of the infant cranium. Some parents think that 3D CT imaging is not a suitable method because of other potential problems introduced by radiation[12–14]. The handheld-based structured light scanner has high measurement accuracy, but there are still some problems such as high cost, low measurement speed, and its inability to realize single-shot 360-degree measurement [15–18]. Therefore, there is an urgent need for a rapid, accurate, and low-cost 360-degree cranial deformity detection method and its system.

To solve the problems above, this paper proposes a single-shot 360-degree cranial deformity detection system using digital image correlation (DIC). Considering the cost of the hardware system and the efficiency of 360-degree imaging, two plane mirrors are introduced into a stereo 3D DIC measurement system for forming three DIC systems simultaneously including a real system and two virtual systems which are reflected by plane mirrors. The 360-degree speckle images of the infants' cranium can be captured using only one stereo camera. Then, DIC is exploited to calculate the global corresponding relationship of the measured surface under different perspectives to achieve the single-shot 3D profile measurement. With the help of the reflection matrix of plane mirrors, the conversion relationship of 3D point cloud between different DIC systems can be obtained to realize the single-shot 360-degree 3D measurement of the infants' cranium. Finally, the experimental results show that the performance and measurement accuracy of the sys-

tem are proved to meet the requirements of cranial deformity detection.

## 2 Principle

In this section, by introducing plane mirrors into a stereo 3D DIC measurement system, the proposed method consists of the following two parts: single-shot 3D measurement using DIC and 360-degree 3D measurement based on plane mirrors.

### 2.1 Single-Shot 3D Measurement Using DIC

In DIC, the measured object surface is required to have rich texture information. For untextured objects, a random speckle pattern is artificially sprayed or projected onto the tested surface [19–21]. In our method, a speckle pattern is printed to generate a dense and high-quality speckle head cap that increases the feature texture of the infants' cranium. In 3D DIC, two cameras are used to synchronously capture stereo speckle images of the measured object (including reference images and target images). DIC is exploited to calculate the global corresponding relationship of the measured surface under different perspectives to obtain the disparity map, achieving 3D profile and deformation measurement [22–25].

DIC is a matching method based on local windows to estimate the similarity between the reference subset and the target subset. Taking into account the difference in different perspectives, a second-order shape function is introduced to estimate the pixel-wise correspondence between the reference subset and the target subset to achieve a more accurate estimation of the surface deformation:

$$\begin{bmatrix} x' \\ y' \end{bmatrix} = \mathbf{W}(x, y; \mathbf{p}) \begin{bmatrix} x^2 \\ xy \\ y^2 \\ x \\ y \\ 1 \end{bmatrix} \quad (1)$$

$$\mathbf{W}(x, y; \mathbf{p}) = \begin{bmatrix} \frac{u_{xx}}{2} & u_{xy} & \frac{u_{yy}}{2} & 1 + u_x & u_y & u \\ \frac{v_{xx}}{2} & v_{xy} & \frac{v_{yy}}{2} & 1 + v_x & v_y & v \end{bmatrix} \quad (2)$$

where  $\mathbf{p}$  is the deformation parameter of the target subset,  $\mathbf{W}(x, y; \mathbf{p})$  is the shape function of the target subset,  $u_{xx}$ ,  $u_{xy}$ ,  $u_{yy}$ ,  $v_{xx}$ ,  $v_{xy}$ , and  $v_{yy}$  represent the second-order gradient of disparity in the corresponding direction respectively.

At present, the DIC technique based on the inverse compositional Gauss-Newton algorithm (IC-GN) proposed by Pan et al. [26] is a fast, robust, and accurate full-field displacement measurement method, which eliminates the complex redundant calculation involved in traditional DIC without sacrificing its sub-pixel matching accuracy. In IC-GN, the ZNSSD criterion is adopted to estimate the similarity between the reference subset and the target subset

$$C_{\text{ZNSSD}}(\Delta\mathbf{p}) = \sum_{x, y=-M}^M \left\{ \frac{f(\mathbf{W}(x, y; \Delta\mathbf{p})) - \bar{f}}{\Delta f} - \frac{g(\mathbf{W}(x, y; \mathbf{p})) - \bar{g}}{\Delta g} \right\}^2 \quad (3)$$

$$\Delta f = \sqrt{\sum_{x, y=-M}^M [f(\mathbf{W}(x, y; \Delta\mathbf{p})) - \bar{f}]^2} \quad (4)$$

$$\Delta g = \sqrt{\sum_{x, y=-M}^M [g(\mathbf{W}(x, y; \mathbf{p})) - \bar{g}]^2} \quad (5)$$

where  $\Delta\mathbf{p}$  is the increment of deformation parameter,  $\mathbf{W}(x, y; \Delta\mathbf{p})$  is the increment of shape function.  $\bar{f}$  and  $\bar{g}$  are the mean values of reference subset and target subset respectively. In order to solve  $\mathbf{W}(x, y; \Delta\mathbf{p})$ , according to the least-squares algorithm, let it be

$$\frac{\partial C_{\text{ZNSSD}}(\Delta\mathbf{p})}{\partial \Delta\mathbf{p}} = 0 \quad (6)$$

The matching strategy of the IC-GN algorithm is as follows

$$\mathbf{W}(x, y; \mathbf{p}) = \mathbf{W}(x, y; \mathbf{p})\mathbf{W}^{-1}(x, y; \Delta\mathbf{p}) \quad (7)$$

In each iterative of the IC-GN algorithm, the convergence condition is as follows

$$\|\Delta\mathbf{p}\| = \|\mathbf{p}^{n+1} - \mathbf{p}^n\| \leq 10^{-3} \quad (8)$$

After obtaining the high-precision disparity estimation of seed points, multi-thread accelera-

tion is used to implement the reliability-guided full-field matching method to complete the fast global disparity estimation of the measured object, thus realizing the single-shot 3D measurement.

## 2.2 360-Degree 3D Measurement Based on Plane Mirrors

By introducing the plane mirrors into the 3D measurement system, the real 3D data and the virtual 3D data reflected by the plane mirrors can be obtained simultaneously to achieve 360-degree 3D measurement [27]. According to the reflection model of plane mirrors as shown in Fig. 1, the virtual 3D data reflected by the plane mirrors can be transformed into real 3D data, which can be expressed as

$$\begin{bmatrix} \mathbf{X}_r \\ 1 \end{bmatrix} = \mathbf{D}_r \begin{bmatrix} \mathbf{X}_v \\ 1 \end{bmatrix} \quad (9)$$

$$\mathbf{D}_r = \begin{bmatrix} \mathbf{I} - 2\mathbf{n}(\mathbf{n})^T & 2d_w\mathbf{n} \\ 0 & 1 \end{bmatrix} \quad (10)$$

where  $\mathbf{D}_r$  represents the reflection matrix of the plane mirrors,  $\mathbf{X}_r$  and  $\mathbf{X}_v$  are the real and virtual 3D points,  $\mathbf{I}$  is the identity matrix with a size of  $3 \times 3$ ,  $\mathbf{n}$  is the normal vector of the plane mirrors, and  $d_w$  is the distance between the plane mirrors and the origin  $\mathbf{O}$  of the real-world coordinate system.

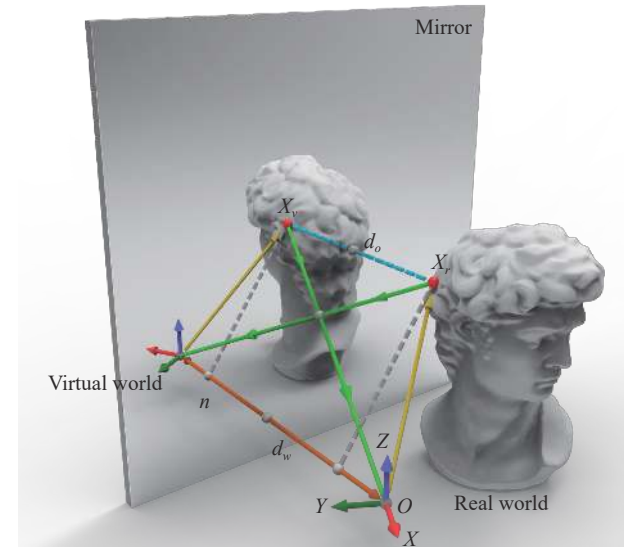


Fig. 1 The schematic diagram of the ideal reflection model for the plane mirror

In order to obtain high-precision model parameters of plane mirrors, the reflection matrix  $\mathbf{D}_r$  (including  $\mathbf{n}$  and  $d_w$ ) is calculated by using the calibration method of plane mirrors based on virtual and real feature point pairs [28]. Firstly, a set of virtual and real feature points are obtained with a circular calibration plate, and their 3D coordinate data are obtained by using the 2D coordinates of the feature points and camera parameters. Assuming that the normal vector  $\mathbf{n}$  is  $(a, b, c)$ , it can be obtained as

$$\begin{cases} [1 - 2a^2]x_v - 2aby_v - 2acz_v + 2ad_w = x_r \\ -2abx_v + [1 - 2b^2]y_v - 2bcz_v + 2bd_w = y_r \\ -2acx_v - 2bcy_v + [1 - 2c^2]z_v + 2cd_w = z_r \end{cases} \quad (11)$$

where  $(x_r, y_r, z_r)$  and  $(x_v, y_v, z_v)$  are the 3D coordinates of the real and virtual feature point  $\mathbf{X}_r$  and  $\mathbf{X}_v$ . Through elimination, it can be obtained as

$$\begin{bmatrix} y_v - y_r & x_r - x_v & 0 \\ z_v - z_r & 0 & x_r - x_v \\ 0 & z_v - z_r & y_r - y_v \end{bmatrix} \begin{bmatrix} a \\ b \\ c \end{bmatrix} = 0 \quad (12)$$

The initial guess of  $\mathbf{n}$  is a least-squares minimization problem. Singular value decomposition (SVD) is used to obtain the exact solution of  $\mathbf{n}$ . And then, Eq. (11) can be rewritten for estimating the initial guess of  $d_w$ . Take the first-order derivative equation of Eq. (11) (i.e.,  $f'(d_w) = 0$ ), and the initial value of  $d_w$  can be obtained. Finally, Eq. (11) can be rewritten again based on the Levenberg-Marquardt algorithm as

$$\sum_{n=1}^N g_1^2(\mathbf{G}) + g_2^2(\mathbf{G}) + g_3^2(\mathbf{G}) \quad (13)$$

$$g_1(\mathbf{G}) = (1 - 2a^2)x_v - 2aby_v - 2acz_v + 2ad_w - x_r \quad (14)$$

$$g_2(\mathbf{G}) = -2abx_v + (1 - 2b^2)y_v - 2bcz_v + 2bd_w - y_r \quad (15)$$

$$g_3(\mathbf{G}) = -2acx_v - 2bcy_v + (1 - 2c^2)z_v + 2cd_w - z_r \quad (16)$$

where  $\mathbf{G} = \{a, b, c, d_w\}$ . The minimization of Eq. (13) is a nonlinear least-squares problem, which can be solved by the Levenberg-Marquardt method. After obtaining the reflection matrix  $\mathbf{D}_r$  (including  $\mathbf{n}$  and  $d_w$ ), the conversion relationship

between the two virtual stereo DIC coordinate systems formed by the reflection of the plane mirrors and the real stereo DIC coordinate system can be calculated, thus achieving 360-degree 3D measurement.

### 3 Experiments

In the experimental section, a single-shot 360-degree deformity detection system for infant cranium based on plane mirrors is built to verify the actual performance of the proposed method in Fig. 2. This system includes a stereo camera composed of two monochrome cameras (DMK 33UP1300 with the resolution of  $1280 \times 1024$ ), and two plane mirrors with the front surface reflection (the size of  $30 \text{ cm} \times 30 \text{ cm}$ ) which are placed behind the measured scenes.

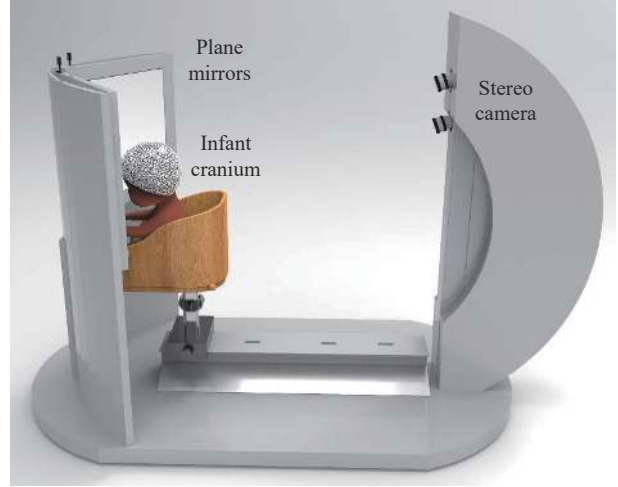


Fig. 2 The diagram of the single-shot 360-degree deformity detection system for infant cranium based on plane mirrors

Before the 360-degree 3D measurement and analysis of the infant cranium, the calibration parameters of the stereo camera and reflection matrixes of plane mirrors are needed. The calibration of the stereo camera can be achieved by capturing the images of the calibration plane in different attitudes. The 3D coordinates of real feature points can be obtained by extracting their 2D coordinates in the calibration plane combined with the parameters of the stereo camera.

And then the 3D coordinates of virtual feature points can be obtained in the same way to form the 3D feature point pairs. The high-precision reflection matrixes of plane mirrors can be calcu-

lated according to the calibration method in Section 2.2. Finally, the 360-degree 3D measurement of the infant cranium can be completed only through the three steps as shown in Fig. 3.

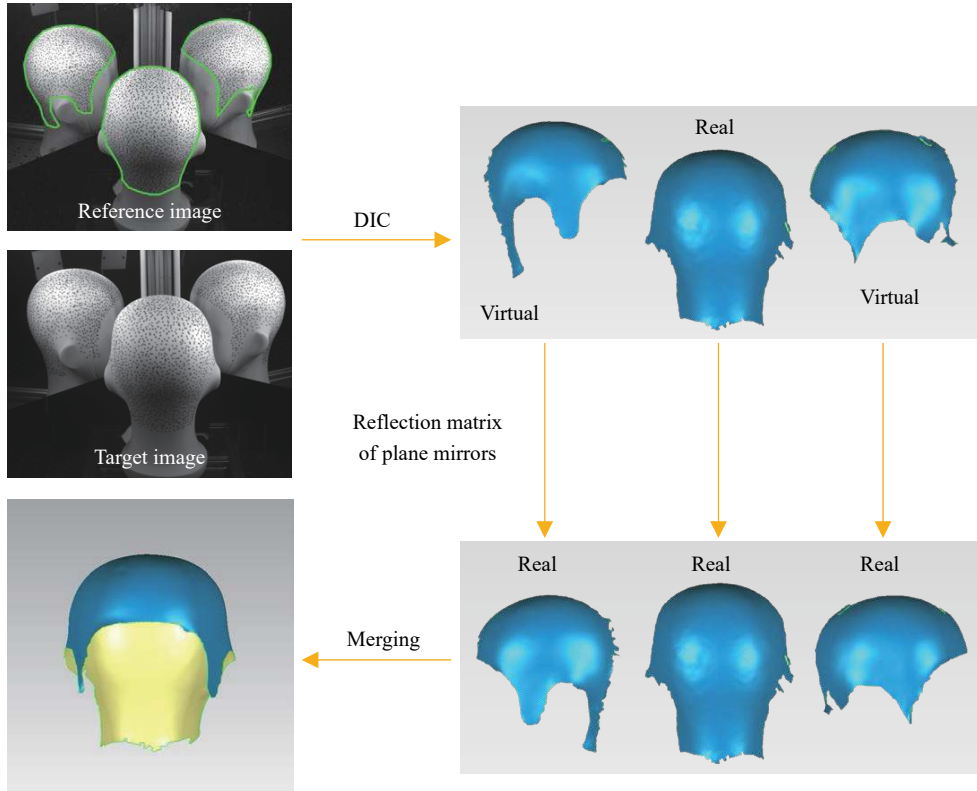


Fig. 3 The flow chart of 3D measurement for the infant cranium

Step 1: The designed speckle pattern is printed on the head cap, and 360-degree stereo speckle images of the infant cranium are captured by the stereo camera.

Step 2: The DIC processes on 360-degree stereo speckle images from three perspectives are independently taken to obtain multi-view 3D surface data of infant cranium at the same time.

Step 3: According to the reflection matrixes of plane mirrors, the real 3D data and virtual 3D data reflected by the plane mirrors can be converted simultaneously to achieve the single-shot 360-degree 3D measurement of the infant cranium.

In order to verify the performance of single-shot 360-degree 3D measurement based on the proposed system, the cranial model was meas-

ured in Fig. 4(a). Taking the real perspective as an example, the region of interest (ROI) to be measured in the reference speckle image was selected manually, and its center point was used as the initial seed point. Then, according to the DIC technique in Section 2.1, the horizontal and vertical disparity map under the real perspective were obtained quickly as shown in Fig. 4(b). Similarly, the disparity map corresponding to the two virtual perspectives can be obtained as shown in Fig. 4(b), achieving the single-shot 360-degree 3D measurement of infant cranium, as shown in Fig. 4(c) and Figs. 5(a)-5(c).

For precision analysis of 3D measurement results, the ground truth of the cranial model is generated via OKIO-5M, an industrial 3D scanning technology. The precision of the OKIO-5M

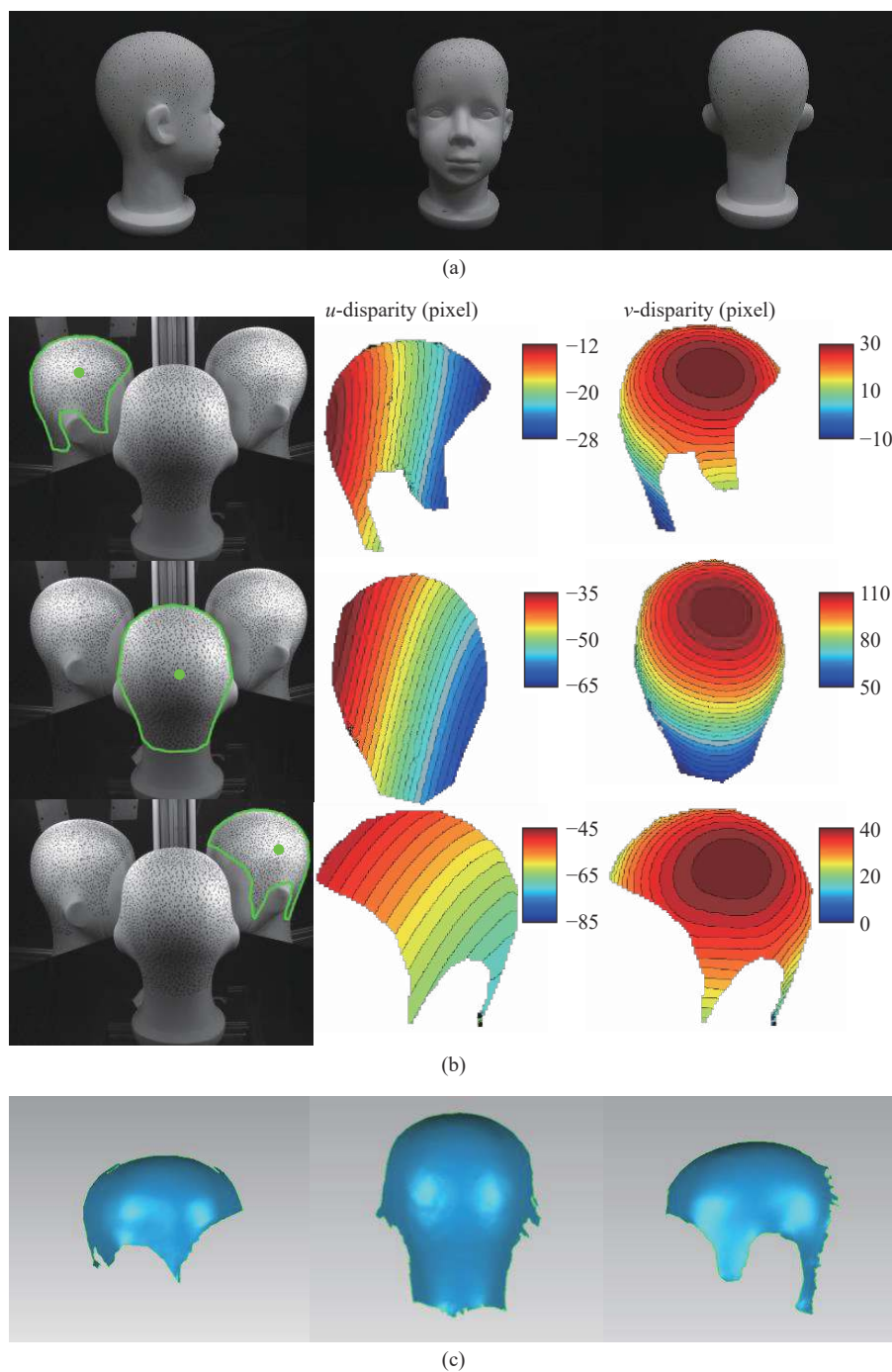


Fig. 4 The single-shot 3D measurement using DIC under three perspectives: (a) three views of the cranial model; (b) the disparity maps in real and virtual perspectives; (c) 3D measurement results under three perspectives

scanner is up to 0.005 mm, as shown in Figs. 5(d)-5(f). Through the point cloud registration algorithm, the differences between the measured data and the ground truth under three single perspectives are shown in Figs. 5(g)-5(i), and the RMS of the measurement errors are 218.64  $\mu\text{m}$ , 118.56  $\mu\text{m}$ , and 224.55  $\mu\text{m}$  respectively. The differences between the combined 360-degree 3D

data from three perspectives and the ground truth are shown in Figs. 5(j)-5(l). The experimental results proved that the proposed system can achieve a single-shot 360-degree measurement with an accuracy of 231.22  $\mu\text{m}$ , and the high-precision 360-degree 3D data of infant cranium can be obtained quickly.

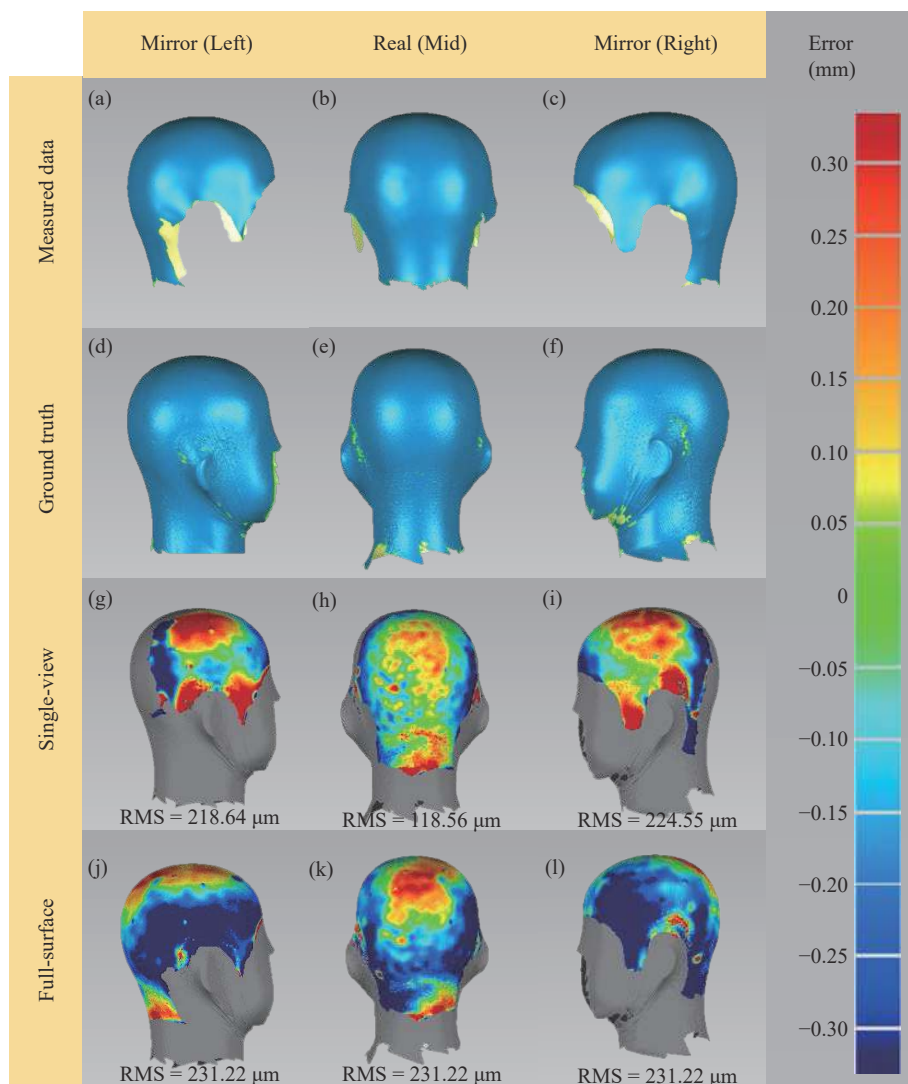


Fig. 5 The precision analysis of the cranial model

## 4 Conclusion

In this paper, a single-shot 360-degree cranial deformity detection system using DIC is proposed to realize rapid diagnosis of cranial deformity. Firstly, a speckle pattern is printed to generate a dense speckle head cap that increases the feature texture of the infants' cranium. Combined with the DIC method based on multi-thread acceleration, the matching accuracy of full-field displacement measurement is improved to realize fast and single-shot 3D measurement with an accuracy of 118.56  $\mu\text{m}$ . Then, the calibration method of plane mirrors based on virtual and real feature point pairs is used to obtain the high-precision point cloud conversion relationship between

different DIC systems, so as to realize a single-shot 360-degree 3D measurement of infant cranium with an accuracy of 231.22  $\mu\text{m}$ . The experiments of 3D measurement and precision analysis of infant cranial models proved that the measurement performance and accuracy of the proposed system meet the medical requirements of infant cranial deformity detection, realizing a rapid, effective, and low-cost infant cranial deformity diagnosis.

## References:

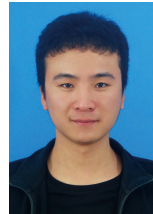
- [1] L. C. Argenta, L. R. David, J. A. Wilson, and W. O. Bell, "An increase in infant cranial deformity with supine sleeping position," *The Journal of Craniofacial Surgery*, vol. 7, no. 1, pp. 5-11, 1996.

- [2] J. Nuysink, M. J. Eijssermans, I. C. van Haastert, C. Koopman-Esseboom, P. J. Helders, L. S. de Vries, and J. van der Net, "Clinical course of asymmetric motor performance and deformational plagiocephaly in very preterm infants," *The Journal of Pediatrics*, vol. 163, no. 3, pp. 658-665, 2013.
- [3] P. Meyer-Marcotty, F. Kunz, T. Schweitzer, B. Wachter, H. Böhm, N. Waßmuth, and C. Linz, "Cranial growth in infants- a longitudinal three-dimensional analysis of the first months of life," *Journal of Cranio-Maxillofacial Surgery*, vol. 46, no. 6, pp. 987-993, 2018.
- [4] M. Zonenshayn, E. Kronberg, and M. M. Souweidane, "Cranial index of symmetry: an objective semiautomated measure of plagiocephaly," *Journal of Neurosurgery: Pediatrics*, vol. 100, no. 5, pp. 537-540, 2004.
- [5] Y. Aihara, K. Komatsu, H. Dairoku, O. Kubo, T. Hori, and Y. Okada, "Cranial molding helmet therapy and establishment of practical criteria for management in Asian infant positional head deformity," *Child's Nervous System*, vol. 30, no. 9, pp. 1499-1509, 2014.
- [6] L. G. Branch, K. Kesty, E. Krebs, L. Wright, S. Leger, and L. R. David, "Deformational plagiocephaly and craniosynostosis: trends in diagnosis and treatment after the 'back to sleep' campaign," *Journal of Craniofacial Surgery*, vol. 26, no. 1, pp. 147-150, 2015.
- [7] A. Binkiewicz-Glińska, A. Mianowska, M. Sokołów, A. Reńska, K. Ruckeman-Dziurdzińska, S. Bakula, and E. Kozłowska, "Early diagnosis and treatment of children with skull deformations. the challenge of modern medicine," *Dev Period Med*, vol. 20, no. 4, pp. 289-295, 2016.
- [8] J. P. Steinberg, R. Rawlani, L. S. Humphries, V. Rawlani, and F. A. Vicari, "Effectiveness of conservative therapy and helmet therapy for positional cranial deformation," *Plastic and Reconstructive Surgery*, vol. 135, no. 3, pp. 833-842, 2015.
- [9] T. Graham, B. Adams-Huet, N. Gilbert, K. Witthoff, T. Gregory, and M. Walsh, "Effects of initial age and severity on cranial remodeling orthotic treatment for infants with deformational plagiocephaly," *Journal of Clinical Medicine*, vol. 8, no. 8, pp. 1097, 2019.
- [10] F. Kunz, T. Schweitzer, J. Kunz, N. Waßmuth, A. Stellzig-Eisenhauer, H. Böhm, P. Meyer-Marcotty, and C. Linz, "Head orthosis therapy in positional plagiocephaly: Influence of age and severity of asymmetry on effect and duration of therapy," *Plastic and Reconstructive Surgery*, vol. 140, no. 2, pp. 349-358, 2017.
- [11] J. P. Stolovitzky and N. W. Todd, "Head shape and abnormal appearance of tympanic membranes," *Otolaryngology—Head and Neck Surgery*, vol. 102, no. 4, pp. 322-325, 1990.
- [12] A. Katsumata, M. Fujishita, M. Maeda, Y. Ariji, E. Ariji, and R. P. Langlais, "3D-CT evaluation of facial asymmetry," *Oral Surgery, Oral Medicine, Oral Pathology, Oral Radiology, and Endodontology*, vol. 99, no. 2, pp. 212-220, 2005.
- [13] L. A. Fox, M. W. Vannier, O. C. West, A. J. Wilson, G. A. Baran, and T. K. Pilgram, "Diagnostic performance of CT, MPR and 3DCT imaging in maxillofacial trauma," *Computerized Medical Imaging and Graphics*, vol. 19, no. 5, pp. 385-395, 1995.
- [14] E. Bo, X. Ge, Y. Luo, X. Wu, S. Chen, H. Liang, S. Chen, X. Yu, P. Shum, and J. Mo, "Cellular-resolution in vivo tomography in turbid tissue through digital aberration correction," *Photonix*, vol. 1, no. 1, pp. 1-12, 2020.
- [15] S. S. Gorthi and P. Rastogi, "Fringe projection techniques: whither we are?," *Optics and Lasers in Engineering*, vol. 48, pp. 133-140, 2010.
- [16] C. Zuo, S. Feng, L. Huang, T. Tao, W. Yin, and Q. Chen, "Phase shifting algorithms for fringe projection profilometry: A review," *Optics and Lasers in Engineering*, vol. 109, pp. 23-59, 2018.
- [17] W. Yin, S. Feng, T. Tao, L. Huang, M. Trusiak, Q. Chen, and C. Zuo, "High-speed 3D shape measurement using the optimized composite fringe patterns and stereo-assisted structured light system," *Optics Express*, vol. 27, no. 3, pp. 2411-2431, 2019.
- [18] W. Yin, C. Zuo, S. Feng, T. Tao, Y. Hu, L. Huang, J. Ma, and Q. Chen, "High-speed three-dimensional shape measurement using geometry-constraint-based number-theoretical phase unwrapping," *Optics and Lasers in Engineering*, vol. 115, pp. 21-31, 2019.
- [19] Y. Dong and B. Pan, "A review of speckle pattern fabrication and assessment for digital image correlation," *Experimental Mechanics*, vol. 57, no. 8, pp. 1161-1181, 2017.
- [20] G. Bomarito, J. Hochhalter, and T. Ruggles, "Development of optimal multiscale patterns for digital image correlation via local grayscale variation,"

- Experimental Mechanics*, vol. 58, no. 7, pp. 1169-1180, 2018.
- [21] B. Pan, "Digital image correlation for surface deformation measurement: Historical developments, recent advances and future goals," *Measurement Science and Technology*, vol. 29, no. 8, pp. 082001, 2018.
- [22] K. Genovese and D. Sorgente, "A morphing-based scheme for large deformation analysis with stereodic," *Optics and Lasers in Engineering*, vol. 104, pp. 159-172, 2018.
- [23] Z. Hu, H. Xie, J. Lu, H. Wang, and J. Zhu, "Error evaluation technique for three-dimensional digital image correlation," *Applied Optics*, vol. 50, no. 33, pp. 6239-6247, 2011.
- [24] Z. Tang, J. Liang, Z. Xiao, and C. Guo, "Large deformation measurement scheme for 3D digital image correlation method," *Optics and Lasers in Engineering*, vol. 50, no. 2, pp. 122-130, 2012.
- [25] X. Shao, X. Dai, Z. Chen, and X. He, "Real-time 3D digital image correlation method and its application in human pulse monitoring," *Applied Optics*, vol. 55, no. 4, pp. 696-704, 2016.
- [26] B. Pan, K. Li, and W. Tong, "Fast, robust and accurate digital image correlation calculation without redundant computations," *Experimental Mechanics*, vol. 53, no. 7, pp. 1277-1289, 2013.
- [27] G. L. Mariottini, S. Scheggi, F. Morbidi, and D. Prattichizzo, "Planar mirrors for image-based robot localization and 3D reconstruction," *Mechatronics*, vol. 22, no. 4, pp. 398-409, 2012.
- [28] W. Yin, S. Feng, T. Tao, L. Huang, S. Zhang, Q. Chen, and C. Zuo, "Calibration method for panoramic 3D shape measurement with plane mirrors," *Optics Express*, vol. 27, no. 25, pp. 36538-36550, 2019.



**Shaogang Liu** is currently pursuing a master's degree in Instrumentation Engineering at Nanjing University of Science and Technology. His research interest is mainly focused on optical 3D measurement.



**Long Yin** is currently pursuing his B.E. degree in Opto-Electronic Information Science and Engineering at Nanjing University of Science and Technology. His research interest is mainly focused on optical 3D measurement.



**Wei Yin** joined the School of Electronic and Optical Engineering at Nanjing University of Science and Technology as a postdoctoral researcher in 2022. His research interests include high-speed 3D measurement based on fringe projection, fast real-time 3D measurement based on speckle projection, stereo vision, and deep learning.



**Yuzhen Zhang** has been an associate professor at Nanjing University of Science and Technology since 2003. Her research interests include dynamic optical 3D measurement, image processing, and other directions.



**Chao Zuo** has been a professor and doctoral supervisor at Nanjing University of Science and Technology since 2017. His research interests include optical metrology, digital holography, and quantitative phase imaging.